Mineral chemistry of columbite–tantalite from spodumene pegmatites of Kolmozero, Kola Peninsula (Russia)

E.V. Badanina [a], M.A. Sitnikova [b], V.V. Gordienko [a,1], F. Melcher [b], H.-E. Gäbler [b], J. Lodziak [b], L.F. Syritso [a]

[a] St.Petersburg State University, 7/9 Universitetskaya Emb., 199034 St. Petersburg, Russia
[b] Federal Institute for Geosciences and Natural Resources (BGR), Stilleweg 2, D-30655 Hannover, Germany

ARTICLE INFO

ABSTRACT

Compositional variation (results of electron microprobe analyses and mass-spectrometry analyses) of columbite-group minerals (CGM) from fully differentiated albite–spodumene pegmatites at Kolmozero in the Kola Peninsula is evaluated. Concentric zoning, typical of rare-metal pegmatites, was not observed in the Kolmozero pegmatites. Columbite-group minerals occur in all main parageneses of the pegmatites and form four generations, reflecting the sequence of pegmatite formation. These minerals demonstrate wide variations in the content of major and trace elements. The composition of CGM ranges from columbite-(Fe) to tantalite-(Mn). Fractionation trends were observed in Mn/(Mn + Fe) versus Ta/(Ta + Nb) diagrams and trace-element abundances plotted versus XTa and XMn. The early CGM paragenesis is characterized by homogeneous, oscillatory and progressive oscillatory zoning and corresponds to a primary magmatic type. Late-generation CGM show patchy irregular internal textures replacing earlier regular patterns of zoning. The irregular zoning points to metasomatic replacement processes. For the first time, it is shown that distributions of rare earth elements (REE) in CGM reflect the evolution of a pegmatite-forming system. At Kolmozero, the main trend of REE variation from early to late generations of CGM involves decreasing total REE contents due to a decrease in heavy REE and Y, decreasing negative Eu anomaly and decreasing magnitude of M-shape tetrad effect between Gd and Ho. These changes are accompanied by gradual flattening of the "bird-like" patterns of chondrite-normalized REE distribution. All these features are typical for late differentiates of granitic volatile-rich magma. Late metasomatic tantalite-(Mn) is characterized by sharp changes in its REE distribution pattern: decreasing total REE contents, changing shape of the REE distribution pattern, the absence of Eu anomaly and tetrad effects, and the appearance of a negative Ce anomaly. The textural characteristics and mineral chemistry of CGM indicate that the pegmatite-forming system underwent several stages of evolution. The earliest magmatic stage can be divided into two sub-stages, involving direct crystallization and collective recrystallization, respectively, and was succeeded by a late hydrothermal–metasomatic post-magmatic stage. Variations in chemical composition among the different generations of CGM are explained by the interplay of several processes: fractional crystallization; competitive crystallization of main rock-forming (feldspar, muscovite, spodumene) and accessory (triphylyte–lithiophilite, spessartine, fluorapatite, zircon, microlite) minerals; and evolution of the mineral-forming environment from a melt to a hydrothermal–metasomatic fluid.

1 . Introduction

Despite the vast amount of literature on the internal structure, mineralogy and petrogenesis of rare-metal granitic pegmatites, the processes leading to the development of Ta mineralization in these rocks are still not completely understood (Aurisicchio et al., 2002; Beurlen et al., 2008; Černý, 1989; Černý and Ercit, 1985, 1989; Černý et al., 1986, 1992, 2004, 2007; Ercit et al., 1995; London, 2008; Novak and Černý, 1998; Novak et al., 2003; Spilde and Schearer, 1992; Uher et al., 1998). The major problem is to distinguish between primary magmatic columbite–tantalite and secondary hydrothermal–metasomatic ores (Van Lichtervelde et al.,

2007). The Kolmozero pegmatite field in the Kola Peninsula seems a perfect study area to tackle this problem. Here, the pegmatites are characterized by a complex multistage formation history and enrichment in rare metals, including Li, Be, Ta and Nb (Gordienko, 1970). Columbite-group minerals (CGM), whose simplified formula can be expressed as [A](Fe, Mn)[B](Nb,Ta)$_2$O$_6$ crystallized in all main stages of the pegmatite evolution, thus allowing us to trace the evolution of the pegmatite system on the basis of variations in mineral chemistry of these CGM.

2 . Geological setting of the Kolmozero deposit

The Kolmozero rare metal (spodumene) deposit is situated in the south-eastern part of the Archean Kolmozero–Voronya (also referred to as –Voronja or –Voron'ya) greenstone belt in the Kola Peninsula (Fig. 1).

The long tectonic history of this Archean suture zone (2930–2550 Ma; Pozhilenko et al., 2002) terminated in the formation of a late-orogenic multistage granodiorite–leucogranite complex with associated pegmatites. The geological position and mineralogical–geochemical features of the pegmatites indicate that these rocks are vein analogues of tourmaline–muscovite leucogranite stocks formed in the final evolutionary stage of the Porosozerskii intrusive complex (Gordienko, 1970, 1996; Petrovskii and Vinogradov, 2002). The 2518 ± 9 Ma U–Pb radiometric age of tantalite from the Vasin-Mylk pegmatite deposit in the north-western part of the Kolmozero–Voronya greenstone belt probably reflects the time of pegmatite crystallization, coeval with the age of the tourmaline granites (Kudryashov et al., 2004; Tkachev, 2011).

The pegmatites of the Kolmozero deposit are located in a layered metagabbro–anorthosite intrusion with a north-western trend and concordant to the boundary between volcanic–sedimentary rocks of the greenstone belt and basement granite-gneisses. The pegmatites occur as a system of tabular bodies dipping 40–45° to the southwest. The length of the vein system reaches 4.5 km, whereas the length of separate pegmatite bodies ranges from 100 to 1500 m and their thickness from 5 to 60 m. The pegmatites become scarcer to a depth of 400–500 m until they completely disappear in the bottom part of the metagabbro–anorthosite intrusion (Fig. 2). The pegmatites belong to the albite–spodumene type and are characterized by similar modal mineralogy and similar weakly differentiated internal structures. Only towards the north-western part of the vein system, albite–spodumene pegmatites give way to small bodies of muscovite–feldspar pegmatite. The homogeneity of the modal composition contradicts, at a first glance, their very high level of geochemical fractionation, as indicated by their high Rb content (0.21 wt.%) and low K/Rb ratio (9.9), calculated from the average whole rock composition of many pegmatites from the Kolmozero deposit (Gordienko, 1970).

3 . Mineralogical and petrographic characteristics of the Kolmozero pegmatite

There are three types of pegmatites in the Kolmozero pegmatite field: feldspar, muscovite–feldspar and albite–spodumene types.

Černý (1991) defined pegmatite groups as genetic groups, consisting of several pegmatite bodies characterized by the same origin and emplaced in the same area contemporaneously. According to this author, the Kolmozero pegmatites are one group, but not one field. Gordienko (1996) and other Russian researchers (e.g., Granitic Pegmatites, 1997) use the same criteria to define a pegmatite field. In this paper, we adhere to this latter definition.

Pegmatites of feldspar type are characterized by simple mineralogy and internal structure comprising predominantly potassium feldspar (60–70%, more abundant than plagioclase) and quartz (30–40%). Accessory minerals are represented by biotite, muscovite, schorl, garnet-group minerals, magnetite, ilmenite, rarely beryl, pyrochlore, CGM, Nb-bearing rutile and molybdenite. Pegmatites of muscovite–feldspar type contain up to 12% muscovite, up to 50% potassium feldspar, 25% quartz, 15–30% albite and up to 1% schorl. Accessory minerals are beryl, CGM, apatite and garnet-group minerals. Biotite, chlorite-group minerals and holmquistite occur sporadically in the aplite rim of pegmatite bodies.

Pegmatites of albite–spodumene type consist of 30–35% quartz, 30–35% albite, 10–25% potassium feldspar, 18–20% spodumene and 5–7% muscovite. These pegmatites exhibit a thin aplite rim (0.5–5 cm) normally confined to the contact with their wall-rock. This aplite consists of plagioclase (up to 80%) and quartz (up to 70%). Accessory minerals are biotite, holmquistite, tourmaline, apatite and epidote. Towards the core of the pegmatite body, the aplite zone changes to an intermediate zone composed of a coarse-grained quartz–albite aggregate with a granoblastic texture. The main rock-forming mineral here (up to 70%) is platy albite with a grain size of 0.2–0.5 cm. Anhedral quartz with a grain size of 0.1–0.3 cm composes about 30% of the rock. Potassium feldspar and spodumene are rare here and collectively compose <5% of the rock. Nests and veinlets of saccharoidal albite (up to 70–80%) with a small proportion of fine-grained muscovite and quartz occur in this zone. The composition of the nests and veinlets changes significantly towards the centre of the pegmatite: fine-grained spodumene (up to 40%), potassium feldspar (up to 60%) and saccharoidal quartz (up to 80%) appear. Such aggregates have an aplitic texture (termed "secondary aplite" by Gordienko, 1970) and are characterized by a vein-like
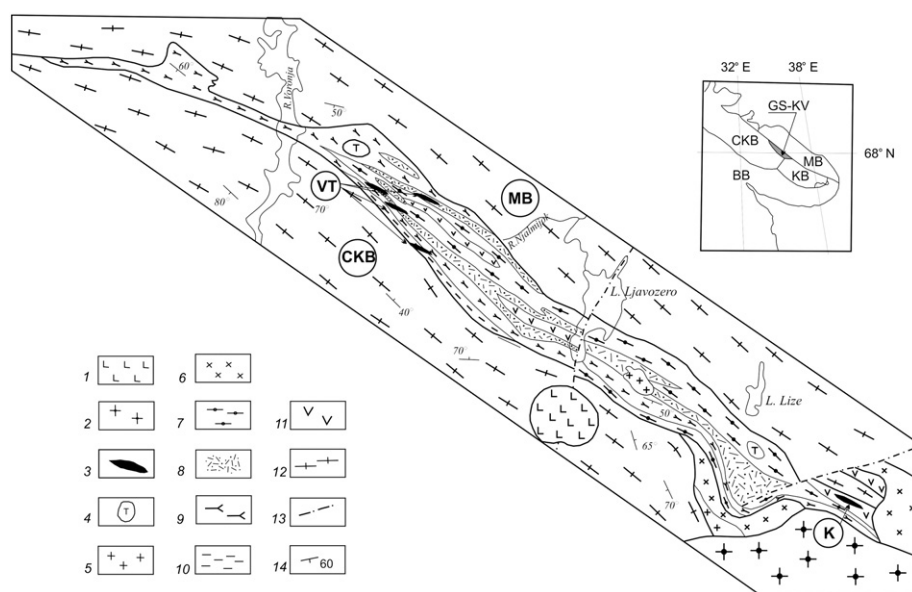

Fig. 1. Sketch map of the Kolmozero–Voronya greenstone belt. 1 — alkaline undifferentiated rocks, Kontozero massif (Devonian); 2 — alkaline granite, West-Keivy massif; 3 — pegmatite of the Kolmozero deposit (K); 4–7 — Porosozerskii intrusive complex: 4 — tourmaline–muscovite leucogranite; 5 — biotite granite; 6 — granodiorite; 7 — metagabbro–anorthosite; 8–10 — volcanic–sedimentary metamorphic rocks of the greenstone belt: 8 — peraluminous gneisses (Chervutskaya formation); 9 — acid volcanic rocks (Voronyinskaya formation); 10 — amphibolites (Polmostundrovskaya formation); 11 — gneisses (Lyavozerskaya formation); 12 — granite–gneisses of the Archean basement; 13 — faults; 14 — structural elements.The inset map shows the location of the Kolmozero–Voronya greenstone belt (GS-KV) between the Murmansk Block (MB), Central-Kola Block (CKB) and Keivy Block (KB); BB — Belomorian Block the term "block" in this context roughly corresponds to "terrain"). VT — Voronyi Tundry pegmatite field (complex pegmatite veins); Vasin–Mylk is situated in the south-eastern part of this field.
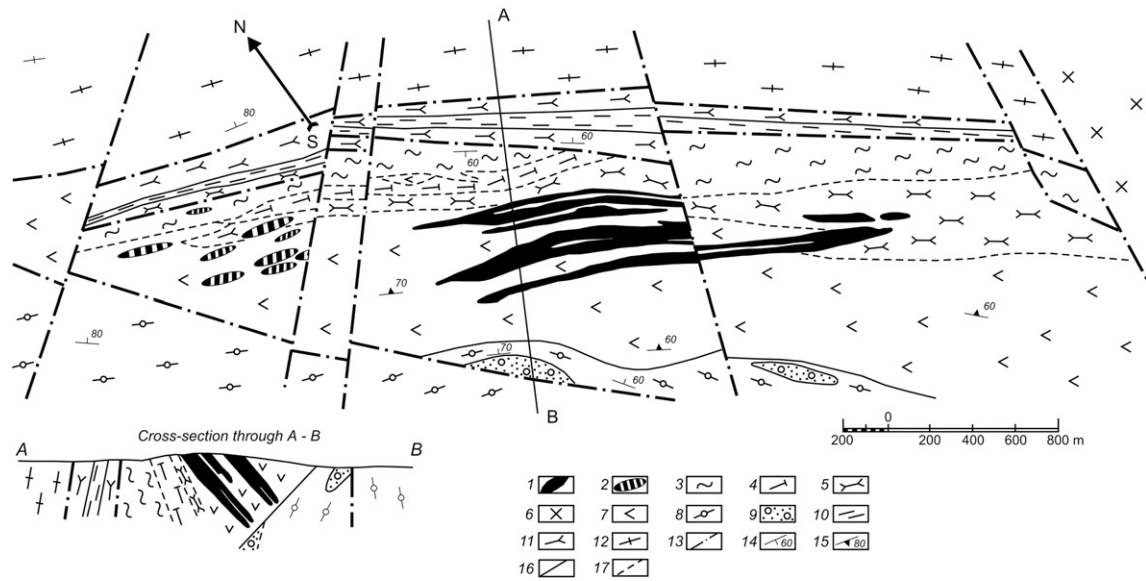
Fig. 2. Geological map of the Kolmozero pegmatite field compiled by Gordienko on the basis of survey data at a scale of 1:5000. 1 — pegmatite of the spodumene type; 2 — pegmatite of muscovite–feldspar type; 3–5 — petrogaphic varieties of metasomatites developed at the expense of gabbro–anorthosites: 3 — quartz–chlorite, 4 — biotite–holmquistite, 5 — amphibole; 6 — granodiorite– gabbro–anorthosite, 8–11 — volcanic–sedimentary complex of the Kolmozero–Voronya greenstone belt: 8 — garnet–biotite gneiss, 9 — conglomerate, 10 — biotite gneiss, 11 — amphibolite; 12 — granite–gneiss of the Archean basement; 13 — faults; 14 — structural elements; 15 — trachytoid structure; 16–17 — geological boundaries: between different metasomatic rocks (16) and between rocks of the volcanic–sedimentary complex.

distribution, diffuse boundaries and a thickness of 0.5–1.2 m. The grain size of the granoblastic aggregate grades from medium- to coarse-grained in the direction from the blocky quartz zone to the spodumene–albite zone. This aggregate forms the bulk volume of the pegmatite veins. The average composition of this pegmatite type is quartz (30%), albite (35%), spodumene (25%) and muscovite (4%).

Macroscopically, this type of pegmatite looks like a mosaic aggregate of quartz and clevelandite-like albite with spodumene crystals developed in-between. The spodumene crystals are oriented sub-perpendicular to the vein contact. In this zone, monomineralic nests of quartz aggregates (up to 3 cm in diameter), albite aggregates (up to 4 cm in diameter) and spodumene (up to 5 cm) occur. The composition of this rock is homogeneous, but in narrow areas, significant fluctuations in spodumene content occur (from 5–10% to 30–50%). In some areas, vein- and nest-like segregations of coarse-grained quartz–muscovite pegmatite from 10 cm to 1 cm in width were observed. Accessory minerals are apatite, spessartine, beryl, CGM, triphylite–lithiophilite and holmquistite. Rare accessory minerals in albite–spodumene pegmatites are microlite, Ta-bearing rutile, zircon, cassiterite and uraninite. Two varieties of microlite are observed: yellow-gray irregular grains up to 0.5 mm in size occurring as overgrowths on CGM, and brown-red octahedral grains up to 0.5 mm in size in the "secondary aplite". The latter variety occurs in interstices among quartz and potassium feldspar grains and was probably formed as a late-stage mineral. Zircon appears as overgrowths on CGM. Rarely, sulfides (sphalerite, pyrite, molybdenite, arsenopyrite), Be silicates (bertrandite, bavenite) and zeolites (chabazite, thomsonite, stilbite-Ca) also occur in this type of pegmatite. Tourmaline-group minerals are quite rare in the albite–spodumene pegmatites, especially in comparison with the feldspar and muscovite–feldspar pegmatites. Isolated schorl crystals up to 2 cm in length occur only in the aplite rim along the pegmatite contact, where they are associated with holmquistite, biotite and epidote. Tourmaline-group minerals are common in the metasomatically reworked wall-rock gabbro-anorthosite. These metasomatic rocks are well studied and described in detail elsewhere (Gordienko et al., 1987).

Concentric zoning, which is common in rare-metal pegmatites, is not observed in the albite–spodumene pegmatites at Kolmozero.

The size of pegmatite bodies increases from the feldspar type to albite–spodumene type. The length of the feldspar pegmatites is tens of meters, rarely up to 150 m at a thickness of <10 m. The length of the muscovite–feldspar veins reaches 100–200 m at a thickness of up to 15 m, and the length of the albite–spodumene-type veins also ranges from 100 to 200 m. The shape of pegmatite bodies does not change visibly with type. In most cases, these rocks occur as tabular bodies, some of which narrow and widen along their strike.

Feldspar-type pegmatites are hosted by amphibole–biotite granodiorite or by biotite- and garnet–biotite gneisses. Those of muscovite–feldspar type are hosted by amphibolite and amphibolite–biotite–garnet gneiss. The pegmatites of albite–spodumene type are hosted only by basic rocks (gabbro–anorthosite and amphibolite).

In the sequence from the feldspar to the muscovite–feldspar to the albite–spodumene pegmatites, the feldspar content progressively decreases. First muscovite and then spodumene become more abundant, which is accompanied by an increase in the proportion of (extremely) coarse-grained mineral aggregates and in the size of pegmatite bodies. All these pegmatite types are characterized by diffuse boundaries among the individual structural zones. Successive transitions from one pegmatite type to another are often observed within a single large pegmatite body along its strike, which implies their genetic relation to one another.

4. Paragenesis

Despite the homogeneity of albite–spodumene pegmatites, their detailed study demonstrates that a great variety of mineral parageneses formed at different stages of their evolution thus arguing for a protracted and complex crystallization history (Gordienko, 1970). The observed paragenetic relationships are generalized in Fig. 3. There are at least four generations of CGM occurring in different parageneses:

The earliest generation to crystallize (CGM-I) forms platy crystals (1–10 mm in size) immersed in a coarse-grained quartz–spodumene–albite aggregate with muscovite making up 70–80 vol.% of the pegmatite body. This generation crystallized later than quartz, spodumene and albite. The crystals are usually found among the grains of silicate minerals, often along cleavage planes in albite and muscovite. This
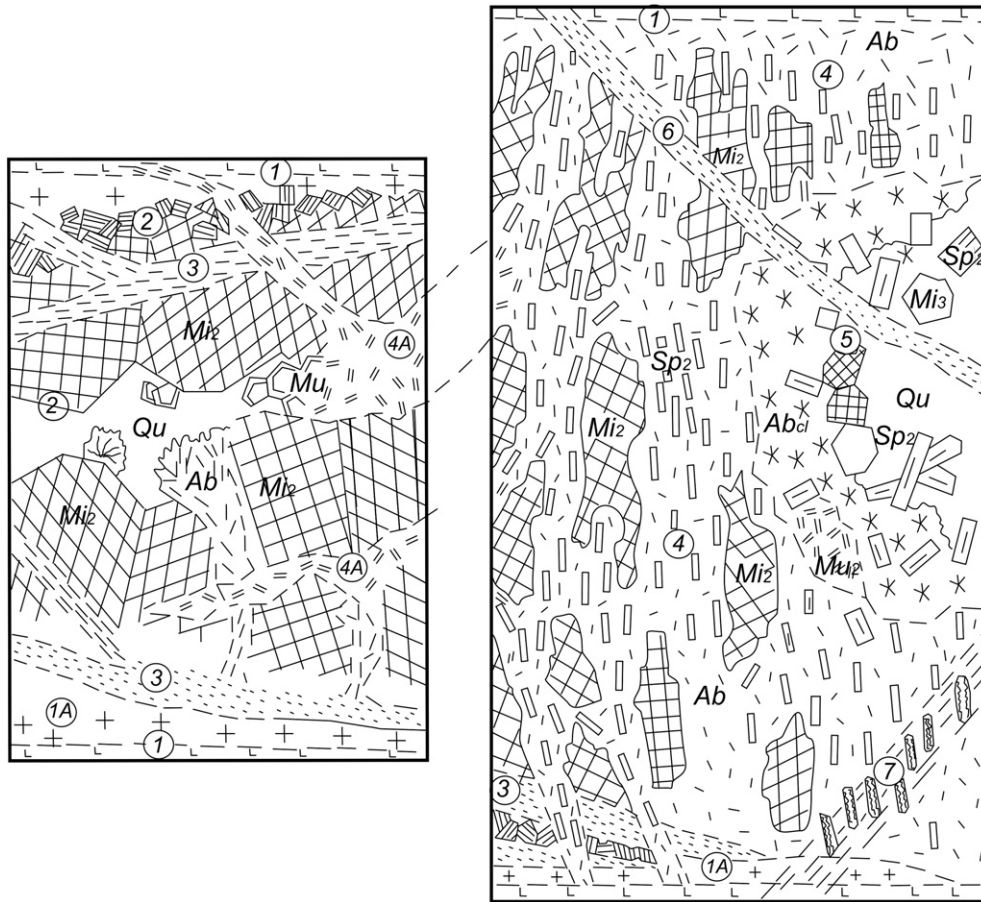
Fig. 3. Internal structure of albite–spodumene pegmatites. 1 — aplite rim; 1A — medium-grained granite; 2 — discontinuous coarse-grained zone of pegmatitic and blocky texture; 3 — fine-grained albite zone; 4 — medium-grained quartz-spodumene – albite pegmatite; 4A — quartz–muscovite pegmatite; 5 — coarse-grained quartz–spodumene–feldspar pegmatite with a blocky texture; 6 — fine-grained albite vein; 7 — fracture zone with leached spodumene (cavernous pegmatite). Qu — quartz; Pl — platy plagioclase; Ab — platy albite, Al_{cl} — platy clevelandite; Mi_2 and Mi_3 — blocky microcline of the second and third generations; Sp_1 and Sp_2 — spodumene of the first and second generations; Mu — muscovite.

generation of CGM is characterized by a very homogeneous distribution within the host aggregate.

The second generation (CGM-II) occurs in two late parageneses: (IIa) platy crystals up to 2 cm across in coarse-grained quartz–muscovite aggregates; and (IIb) thick platy crystals up to 5 cm set in a coarse- to extremely coarse-grained blocky quartz–spodumene–microcline–albite (cleavelandite) aggregates. Accessory minerals found in association with CGM-IIb are spessartine, Mn-bearing apatite and triphylite–lithiophilite group phosphates (Table 1). The parageneses hosting CGM-IIa and -IIb form nests up to 10 m in diameter in coarse-grained albite–spodumene pegmatite.

CGM-III forms platy crystals 1–2 mm in size set in a coarse-grained quartz–muscovite aggregate, whereas CGM-IV is represented by small grains associated with saccharoidal albite and other minerals within the "secondary aplite" (Gordienko, 1970). Some grains of CGM-IV from relatively coarser-grained areas reach 5 mm in size.

5 . Methods

Zoning of CGM was studied using a scanning electron microscope. Representative chemical compositions of CGM from seven samples (from a total of 66 point analyses) are presented in Table 2. The analyses were performed using wavelength-dispersive spectrometry (WDS) with a Cameca SX100 electron microprobe at the Federal Institute for Geosciences and Natural Resources (BGR), Hannover, Germany. The microprobe was operated at 30 kV and 40 nA, and an electron beam diameter of 5 μm. Counting time for Fe, Mn, Nb, Ta, Ti and Sc was 10 s, for W 90 s, for Sn and Zr 100 s and for Hf 120 s. The following natural mineral

and metal standards were used: columbite (Nb Lα), tapiolite (Ta Lα), magnetite (Fe Kα), rhodonite (Mn Kα), scandium (Sc Kα), rutile (Ti Kα), hafnium (Hf Lα), zirconium (Zr Lα), tin (Sn Lα), tungsten (W Lα), and uranium (U Mα). Detection limit for most elements is 200 ppm. Only microprobe analyses with totals between 99 and 101% were used for further interpretation. The mineral formulae of CGM were calculated based on six atoms of oxygen per formula unit (Table 2).

Concentrations of major and selected trace elements in CGM were determined by inductively-coupled-plasma mass-spectrometry and optical emission spectrometry (ICP-MS/ICP-OES) following sample dissolution in acid, or by laser-ablation ICP-MS (LA-ICP-MS) in grain mounts at BGR. Details of the analytical protocols are given in Melcher et al. (2008) and Gäbler et al. (2011). In brief, for the ICP-MS/ICP-OES analysis, 5 to 100 mg of finely ground sample material was dissolved in a mixture of 48% m/m HF and 65% m/m HNO_3, diluted with deionized water and analyzed spectrometrically. For LA-ICP-MS analyses, an excimer 193-nm laser (New Wave UP-193-FX) coupled to a Thermo Scientific ELEMENT XR sector-field ICP-MS instrument was used. The spot diameter was varied between 30 and 50 μm depending on the nature of sample and zoning. Calibration was done by an in-house CGM reference material and glass standard NIST SRM 610.

6 . Results and discussion

6.1. Zoning

Backscattered electron images of CGM from Kolmozero (Fig. 4) highlight variations in Ta/(Ta + Nb) ratio in different zones. There are

Table 1
Representative compositions of Fe–Mn-bearing minerals from the Kolmozero pegmatites (Gordienko, 1970).

wt.%	Biotite 1545	Muscovite-I[a] 9	Muscovite-II[b] 15	Spodumene[c] 1033-e	Spessartine[d] 4000	Triphylite-lithiophilite[e] 1903
SiO$_2$	36.83	44.02	44.04	62.48	35.91	0.90
TiO$_2$	1.66	0.05	0.10	0.06	–	–
Al$_2$O$_3$	16.78	36.38	33.85	26.76	20.12	0.18
Fe$_2$O$_3$	4.03	1.91	3.79	1.18	0.79	1.22
FeO	17.09	0.14	0.10	–	14.34	14.58
MgO	7.65	0.03	0.24	0.21	0.47	0.37
CaO	0.12	0.03	0.26	0.18	0.39	0.75
MnO	0.82	0.04	0.03	0.11	27.66	28.14
K$_2$O	9.12	9.92	9.60	0.08	–	–
Na$_2$O	–	0.66	1.47	0.20	–	3.59
Li$_2$O	0.62	0.09	–	7.57	–	7.95
Rb$_2$O	1.16	0.85	0.75	–	–	–
Cs$_2$O	0.12	0.03	–	–	–	–
SnO$_2$	–	–	–	0.06	–	–
P$_2$O$_5$	–	–	–	–	–	41.53
F	1.08	–	–	–	–	–
Total	100.13	99.28	100.97	98.89	99.68	100.18

[a] Green muscovite-I from a quartz–muscovite aggregate. There are numerous CGM crystals among muscovite grain.
[b] Green muscovite-II from medium to coarse-grained quartz–muscovite–albite pegmatite.
[c] Spodumen from medium-grained quartz–spodumene–albite aggregates with muscovite.
[d] Red-brown spessartine from coarse-grained quartz–spodumene–albite pegmatite.
[e] Greenish-yellow lithiophilite from grayish blocky quartz in association with clevelandite.

several types of zoning in CGM corresponding to different parageneses and generations. Lahti (1987) described three types of zoning in CGM: progressive, oscillatory and patchy, using samples from the Erajärvi granite pegmatites in southern Finland as case example. The same zoning patterns are found in CGM from Kolmozero. Oscillatory zoning is most common. Such zoning can be explained by differences between the rate of attachment of one or more elements to the face of a growing crystal and the rate of diffusion of this element in the mineral-forming environment (Apollonov, 1999). In igneous systems, this type of zoning is caused by mixing of different magmas, rapid cooling, or degassing/

decompression of the system (Holten et al., 1997; Shore and Flowler, 1996).

Less commonly, crystals of CGM-I are fairly homogeneous or show subtle patchy zoning (Fig. 4a). Compositionally heterogeneous crystals, such as that shown in Fig. 4b, contain evidence of secondary alteration, such as darker veinlets (i.e., low in average atomic number, AZ) with bright (high-AZ) minute inclusions of uraninite. The presence of uraninite has important implications for interpretation of post-magmatic events. Some grains are overgrown by a thin (up to 10 μm) rim of Ta-enriched columbite.

Table 2
Selected electron microprobe analyses of columbite-group minerals from the Kolmozero pegmatites (wt.%).

| Element	CGM-I		CGM-IIa		CGM-IIb		CGM-III		CGM-IV			
Sample	1033	1038-2	1012	1012	1013	1013	1022	1022	1607	1607	1067	1067
			Core	Rim	Core	Rim	Irregular zoning	Patchy	Irregular zoning	Patchy	Irregular zoning	Patchy
n[a]	4	7	4	3	16	11	4	2	4	2	4	6
TiO$_2$	0.84	0.57	0.47	0.31	0.51	0.31	0.39	0.10	0.14	0.37	0.24	0.18
MnO	9.46	9.31	8.38	9.94	10.72	10.60	12.96	11.58	11.62	10.78	11.79	13.02
FeO	11.14	10.51	12.27	8.09	8.91	7.22	4.52	3.93	6.45	4.33	6.01	1.38
ZrO$_2$	0.41	0.34	0.06	0.05	0.08	0.09	0.10	<0.01	0.08	0.12	0.05	0.12
Nb$_2$O$_5$	58.16	51.41	56.02	32.77	51.42	35.82	29.77	10.76	34.94	7.57	32.76	3.00
SnO$_2$	0.08	0.11	0.07	0.06	0.07	0.07	0.18	0.04	0.04	0.15	0.07	0.25
Ta$_2$O$_5$	20.34	26.85	21.76	48.20	29.12	46.15	51.17	72.84	46.95	76.20	48.58	81.39
WO$_3$	0.40	0.33	0.33	0.16	0.22	0.17	0.09	<0.01	<0.01	<0.01	<0.01	0.06
Total	100.83	99.43	99.36	99.58	101.05	100.43	99.18	99.26	100.22	99.52	99.50	99.40
Formulae calculated to 6 atoms of O												
Mn	0.486	0.500	0.441	0.590	0.570	0.615	0.783	0.785	0.679	0.741	0.701	0.925
Fe	0.565	0.557	0.638	0.474	0.468	0.414	0.270	0.263	0.372	0.294	0.352	0.097
A site total	1.051	1.057	1.079	1.064	1.038	1.029	1.053	1.048	1.051	1.035	1.053	1.022
Ta	0.335	0.463	0.368	0.918	0.497	0.860	0.993	1.586	0.881	1.680	0.927	1.856
Nb	1.594	1.474	1.574	1.037	1.460	1.109	0.960	0.389	1.090	0.277	1.039	0.114
Sn	0.002	0.005	0.002	0.002	0.002	0.002	0.005	0.001	0.001	0.005	0.002	0.008
Ti	0.038	0.027	0.022	0.016	0.024	0.016	0.021	0.006	0.007	0.023	0.013	0.011
Zr	0.012	0.010	0.002	0.002	0.002	0.003	0.004	<0.001	0.003	0.005	0.002	0.005
W	0.006	0.005	0.005	0.003	0.004	0.003	0.002	<0.001	<0.001	<0.001	<0.001	0.001
B site total	1.987	1.984	1.973	1.978	1.989	1.993	1.985	1.984	1.983	1.910	1.984	1.995
Mn/(Mn + Fe)	0.466	0.476	0.413	0.558	0.552	0.599	0.746	0.751	0.649	0.718	0.668	0.877
Ta/(Ta + Nb)	0.173	0.239	0.189	0.470	0.254	0.437	0.508	0.803	0.447	0.858	0.472	0.942

[a] Number of analyses.
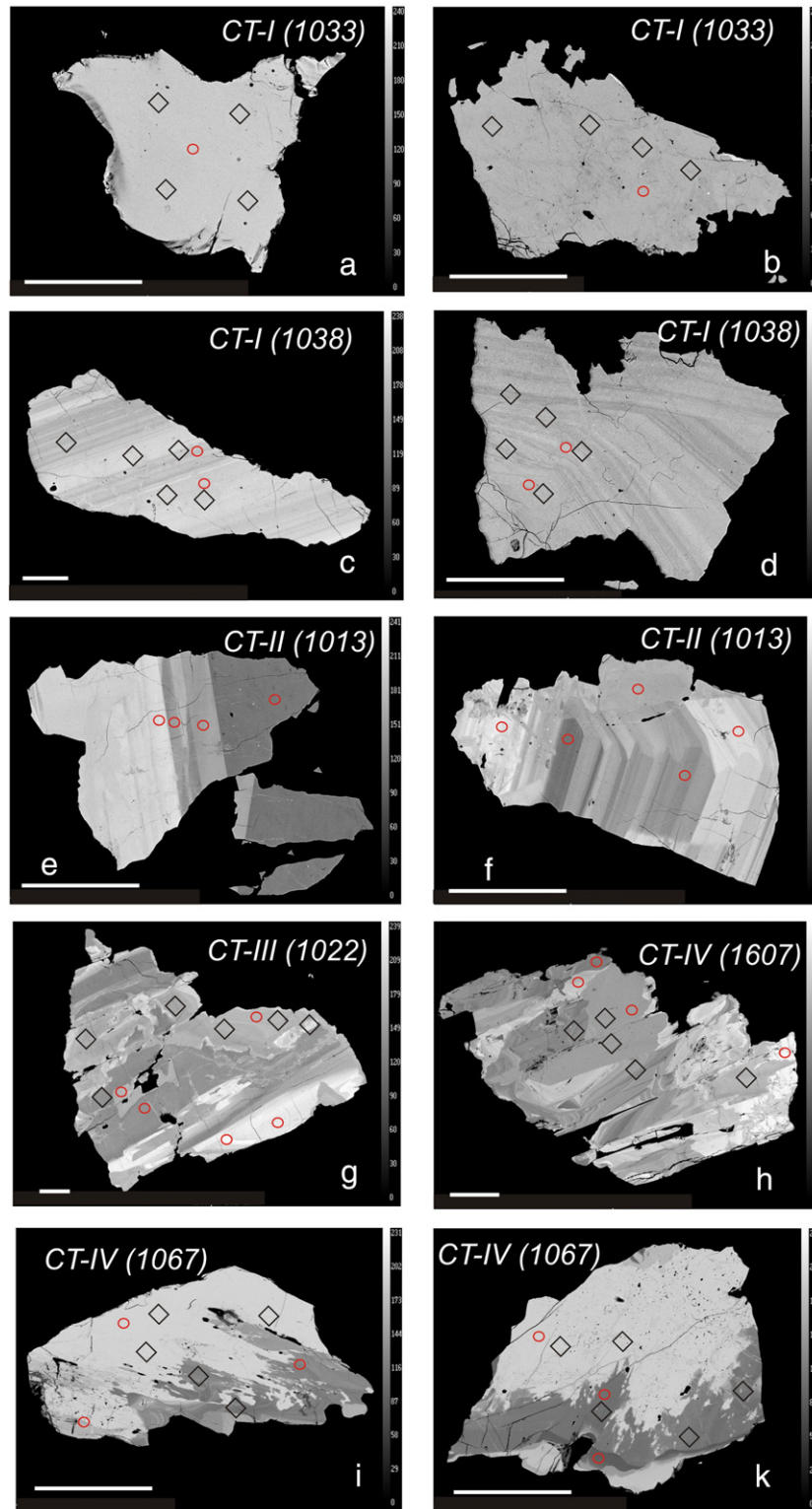
Fig. 4. Zoning patterns of CGM from Kolmozero (BSE images): a) homogeneous crystal; b) blocky pattern; c,d) oscillatory zoning; e) progressive oscillatory zoning, f) juxtaposed progressive oscillatory and sector zoning; g,h) irregular-oscillatory zoning; i,k) patchy overprints on earlier zoning patterns. Scale bar is 500 μm; circles indicate microprobe analyses, diamonds LA-ICP-MS analyses.

A good example of oscillatory zoning is shown in Fig. 4c, d (sample 1038). Usually, individual zones are very thin and parallel to the crystal edges. As mentioned above, this type of zoning probably reflects local fluctuations in the composition of the mineral-forming environment and indicates that the crystal grew under near-equilibrium conditions. Close inspection of many oscillatory-zoned grains (e.g., Fig. 4d) reveals

that the primary zoning was perturbed at later crystallization stages, which we attribute to post-magmatic evolution of the host pegmatite. These textural observations suggest the possibility that even early generations of CGM subsequently underwent alteration. Columbite-(Mn) of generation II (Fig. 4e, f) is characterised by juxtaposed progressive oscillatory zoning and sector zoning. The general compositional trend
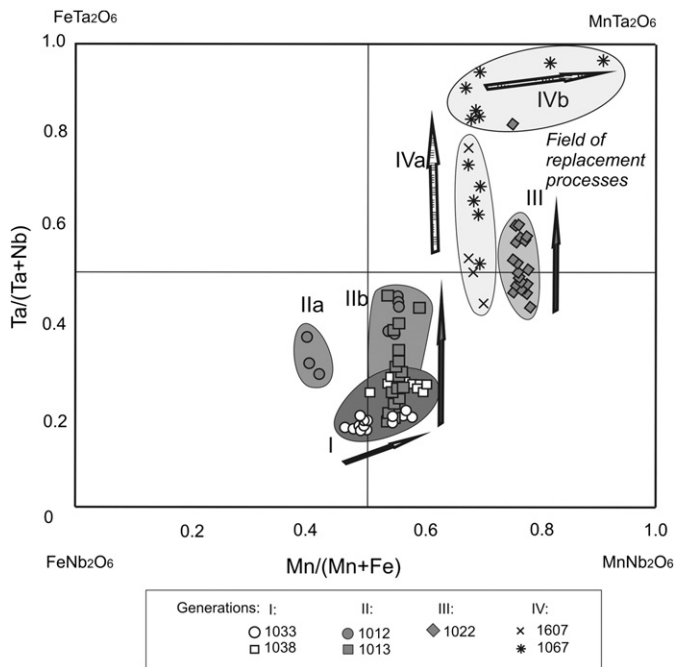
Fig. 5. Compositional evolution of CGM from albite–spodumene pegmatites of the Kolmozero field expressed in terms of Mn/(Mn + Fe) and Ta/(Ta + Nb) atomic values. CGM-I is from quartz–spodumene–albite paragenesis; CGM-II from coarse-grained microcline–spodumene–clevelandite aggregate immersed in blocky quartz; CGM-IIa is relics of columbite-(Fe) in CGM from muscovite paragenesis (sample 1012); CGM-IIb is from muscovite (sample 1012) or albite paragenesis (sample 1013); CGM-III from coarse-gained quartz–muscovite aggregate, CGM-IV from the "secondary aplite" zone (saccharoidalalbite); IVa — from parts with oscillatory zoning; and CGM-IVb is from parts of patchy zoned areas. Arrows show the evolution trends of CGM composition from CGM-I to CGM-IV generation during the pegmatite formation.

for this type of zoning is an increase in Ta content from the crystal core towards its rim. The grain in Fig. 4e is a fragment of a larger crystal with progressive oscillatory zoning.

More complex zoning was observed in CGM-III, such as sample 1022 (Fig. 4g), and can be characterized as irregular oscillatory and patchy. Crystals of the latest generation (CGM-IV) are characterized by patchy zoning (sample 1067) overprinting the earlier irregular oscillatory pattern (Fig. 4h–k) and indicating metasomatic replacement. In Fig. 4k, the large high-AZ region in the upper part of the image shows a number of microveinlets indicative of further alteration. Multiple stages of post-magmatic alteration are reflected in two types of replacement: CGM by CGM, or CGM by other Ta–Nb phases (e.g., microlite), which is typical of late low-temperature parageneses (Černý et al., 1986). The first type of alteration was observed in CGM-IV (Fig. 4i, k), whereas replacement of CGM-IV by microlite was described by Gordienko (1970).

6.2.1. Mineral chemistry of CGM: major elements

Representative compositions of CGM from the albite–spodumene pegmatites of Kolmozero are presented in Table 2. Several evolutionary trends can be identified in a Mn/(Mn + Fe) versus Ta/(Ta + Nb) diagram conventionally used for these purposes (Fig. 5). In this diagram, discrete fields correspond to different CGM generations. Four trends marked by arrows correspond to the four generations of CGM described in Section 4. The composition of CGM-I varies only slightly; in general, it evolves towards higher Mn/(Mn + Fe) ratios (0.4 to 0.6). Progressively zoned CGM-II evolve to Ta-rich varieties [i.e. from Ta/(Ta + Nb) = 0.2 to 0.5]. The cause for variations in Mn/(Mn + Fe) is not quite clear for this generation of CGM. Some analyses of sample 1012 plot within the CGM-IIa field, whereas others plot within the CGM-IIb field. These discrepancies can be explained by some variation in Fe activity in the mineral-forming environment due to competition from Fe-rich

muscovite in the IIa paragenesis (Table 1). We cannot explain the observed fluctuations in Mn content at present because there are no minerals capable of scavenging Mn in this paragenesis. However, CGM-IIb is associated with a number of Mn-rich phases, including spessartine, apatite (up to 5.8 wt.% MnO: Gordienko, 1970) and triphylite–lithiophilite phosphates (up to 35.5 wt.% MnO: Gordienko, 1970); see also Table 1 for representative analyses of some minerals. In CGM-IIa, the Mn/(Mn + Fe) value ranges from 0.4 to 0.5. In CGM-IIb, the Fe and Mn contents remain constant [Mn/(Mn + Fe) = 0.55]. Crystals of CGM-III are very different from CGM-II in both Mn/(Mn + Fe) and Ta/(Ta + Nb) ratios (0.75 and 0.4–0.6, respectively). The main feature of CGM-IVa is an increase of Ta/(Ta + Nb) ratio from 0.4 to 0.8 at a constant Mn/(Mn + Fe) value (~0.65). In contrast, the Mn/(Mn + Fe) value in CGM-IVb varies significantly (from 0.7 to 0.9), but its Ta/(Ta + Nb) ratio remains constant.

The compositional zoning in CGM from the Kolmozero pegmatites corresponds to the major trends recognized by Černý (1989) and Černý et al. (1992) for the lepidolite and spodumene subtypes of rare-metal pegmatites worldwide. With increasing grade of pegmatite fractionation, CGM are progressively enriched in Mn and then Ta. An increase in Ta/(Ta + Nb) ratio during crystallization of the pegmatite with fractionation could be explained by the lower solubility of columbite-(Mn) in peraluminous granite/pegmatite melts (Linnen and Keppler, 1997) in comparison with tantalite-(Mn). In addition, the solubilities of columbite and tantalite increase with increasing temperature and Li content of the melt (Fiege et al., 2011). This trend culminates with late crystallization of tantalite and usually involves decreasing temperature, Li and F contents, leading to the deposition of Li- and F-bearing minerals (spodumene and lepidolite) in central parts of concentrically zoned pegmatite bodies. In accord with this general observation, Ta mineralization is also concentrated near the core of pegmatite bodies in a late magmatic or replacement parageneses. Although Fiege et al. (2011) and Aseri and Linnen (2011) showed that the solubilities of columbite-(Mn) and tantalite-(Mn) in nearly fluid-saturated granitic melts are independent of F concentration in these melts, Fiege et al. (2011, p. 173) concluded that "a complex interaction of e.g. Li, F, B and P may influence the solubility of minerals of the columbite group".

The increase of Mn/(Mn + Fe) ratio in CGM-IV during the pegmatite evolution (Fig. 5) cannot be explained exclusively by fractional crystallization. This trend is typical for CGM developed from the F-rich pegmatite subtype of Černý et al. (1986). Taking into account the higher solubility of columbite-(Fe) in comparison with columbite-(Mn), this trend could indicate that the Fe–Mn balance in the pegmatitic melt was controlled by another Fe–Mn-bearing mineral, such as mica, tourmaline, or garnet during the pegmatite evolution (van Lichtervelde et al., 2006, 2007). In the Kolmozero samples, the most important Fe–Mn silicate host phases are Fe-bearing muscovite, triphylite–lithiophilite phosphates and spessartine, whereas biotite is rare. Schorl is also quite rare and occurs only in the contact aplitic zone. Holmquistite appears only at the contact with the host gabbros and amphibolites. Representative compositions of these minerals are given in Table 1.

During the post-magmatic stage, tantalite-(Mn) crystallizes as an overgrowth and a replacement rim on CGM, reflecting a dramatic increase in Mn concentration in the mineral-forming environment. Černý (1989) suggested that an increase in Ta/Nb ratio is typical of CGM from both primitive Li–F-poor magmas and Li–F-rich melts, but extreme fractionation takes place only in the latter. The evolution of the Fe/Mn budget of CGM, on the contrary, is observed only in systems with a high activity of F during the final stages of granite or pegmatite crystallization. Fluorine is unlikely to play any important role in the Kolmozero pegmatites, as suggested by the very low concentrations of this element. Therefore, the documented changes in Fe/Mn ratio in CGM from Kolmozero most likely arise from an increase in Mn concentration in the course of crystal fractionation, independently of fluorine activity.

Table 3
Representative ICP-MS analyses of trace elements in CGM from the Kolmozero pegmatites, in ppm.

Element	CGM-I		CGM-II						CGM-IV	
	1033	1038-2	1013	1012	1022	1022	1022	1022	1607	1067
Al	885.8	177.5	1399	323.1	586	1028	460.5	416.2	4373	1357
Ti	3779	3345	2373	3455	2358	2313	2184	2559	1463	1383
Li	11.0	20.1	21.9	15.9	10.8	30.6	16.2	16.5	40.9	18.6
Rb	5.099	3.389	34.15	5.039	46.62	30.31	40.69	26.21	70.44	25.96
Sr	bd	15.6	10.4	bd	17.6	57.8	21.7	34	bd	111.6
Ba	bd	bd	bd	bd	bd	bd	bd	bd	64	33
Th	10.22	35.42	15.71	12.23	11.31	14.495	13.96	20.28	6.984	26.03
U	629.7	1202	460.5	539.4	618.3	593.5	699.2	1006	178.1	697.9
Pb	413.9	475	409.8	301.1	313.6	235.5	374.2	495.6	132.1	304.1
Zr	1392	1843	1128	1418	848.7	982.6	1014	1155	559.9	1329
Hf	190.3	286.2	211.4	288.6	143.4	301.5	189.8	181.7	275	629.1
W	3113	2711	1804	2512	2073	1417	1313	1522	734	332
Bi	1.97	31.35	2.76	5.58	0.97	1.28	1.05	0.89	62.94	19.73
As	1.7	3.2	bd	4.2	1.5	3.2	3.9	2.4	bd	6.8
Sb	0.31	1.73	1.36	0.50	1.26	2.23	1.47	1.92	4.22	14.73
Y	12.43	29.55	4.41	3.78	2.16	0.82	2.12	3.08	0.56	1.09
Zr/Hf	7.32	6.44	5.34	4.91	5.92	3.26	5.34	6.36	2.04	2.11
La	1.969	1.561	1.491	0.713	4.273	2.219	4.268	5.404	1.806	0.631
Ce	1.806	0.554	1.409	0.938	6.154	2.974	5.690	7.360	0.908	0.263
Pr	0.167	0.041	0.160	0.105	0.265	0.238	0.237	0.321	0.180	0.092
Nd	0.495	0.139	0.556	0.312	0.606	0.634	0.544	0.764	0.483	0.332
Sm	0.221	0.394	0.226	0.099	0.108	0.123	0.099	0.132	0.103	0.071
Eu	0.013	0.002	0.013	0.010	0.012	0.016	0.012	0.016	0.015	0.019
Gd	0.571	1.663	0.375	0.182	0.140	0.123	0.137	0.184	0.081	0.093
Tb	0.298	0.979	0.130	0.088	0.039	0.026	0.045	0.061	0.016	0.016
Dy	2.448	6.844	0.821	0.693	0.316	0.180	0.354	0.495	0.107	0.096
Ho	0.367	0.699	0.097	0.093	0.045	0.026	0.047	0.064	0.018	0.014
Er	1.470	1.929	0.323	0.343	0.160	0.079	0.156	0.212	0.055	0.043
Tm	0.332	0.357	0.066	0.078	0.034	0.011	0.031	0.043	0.010	0.005
Yb	3.317	3.019	0.669	0.782	0.365	0.085	0.308	0.422	0.073	0.041
Lu	0.548	0.371	0.121	0.121	0.051	0.011	0.041	0.057	0.014	0.008
ΣREE	14.02	18.55	6.455	4.559	12.57	6.745	11.97	15.53	3.870	1.725
$(La/Yb)_n$	0.40	0.35	1.51	0.62	7.96	17.84	9.43	8.69	16.85	10.48
$(Sm/Nd)_n$	1.38	8.74	1.25	0.98	0.55	0.60	0.56	0.53	0.66	0.66
Eu/Eu^*	0.113	0.008	0.134	0.239	0.303	0.402	0.315	0.317	0.519	0.708
T_3	1.07	1.7	0.9	1.11	0.56	0.34	0.74	0.78	0.18	0.19
T_4	0.18	0.25	0.1	0.23	0.29	0.09	0.26	0.27	0.04	0.22

bd — below detection limit.
$Eu/Eu^* = Eu_n/(Sm_n \times Gd_n)^{0.5}$, $(La/Yb)_n$ and $(Sm/Nd)_n$ – ratios normalized to the chondrite values of Sun and McDonough (1989). T_3, T_4 are indicator of the lanthanide tetrad effect defined by Monecke et al. (2002) as follows
$T_i = (0.5 \times (X_{Bi}/(X_{Ai}^{2/3} \times X_{Di}^{1/3}) - 1)^2 + (X_{Ci}/(X_{Ai}^{1/3} \times X_{Di}^{2/3}) - 1)^2))^{0.5}$, where X_{Ai} is the chondrite-normalized concentration of the first, X_{Di} of the last, and X_{Bi}, X_{Ci} are chondrite-normalized concentrations of the middle elements in the tetrad. The T_3 and T_4 values reflect fractionation within the Gd–Ho and Er–Lu tetrad, respectively.

6.2.2. Mineral chemistry of CGM: trace elements

Concentrations of minor elements (Ti, Sn, W and Zr) in the examined CGM do not exceed 1 wt.% respective oxide and are often close to their detection limit by WDS. Therefore, these and a large selection of trace elements were analyzed by ICP-MS. The analytical results are presented in Tables 3 and 4, and the abundances of selected elements are plotted versus the mole fractions of Mn and Ta (XMn and XTa, respectively) in Fig. 6a–c. The major element concentrations analyzed by ICP-OES have been used to confirm the chemical composition of the hand-picked CGM grains only and are not reported in the present work. The XMn and XTa were calculated as follows: $X_{Mn} = 100*Mn/(Mn + Fe)$ and $X_{Ta} = 100*Ta/(Ta + Nb)$, both based on the atomic abundances of the elements.

In-situ analyses by LA-ICP-MS reflect the distribution of trace elements in different zones of the same crystal, whereas the bulk analyses by conventional solution ICP-MS provide insight into element abundances integrated for the whole grain. Obviously, the latter type of analysis does not reflect the complexity of crystallization processes involved in the formation of CGM, or their heterogeneity. This heterogeneity can be quite significant owing to the presence of mineral inclusions (mica, feldspars), as well as effects of post-magmatic recrystallization, alteration and exsolution in the examined material. In the following discussion, we will consider the behavior of trace elements in CGM mainly

on the basis of the in-situ LA-ICP-MS analyses, unless indicated otherwise.

According to the conventional ICP-MS results (Table 3), Rb concentrations continuously increase from the early to late generations of CGM (from 3.4 to 70.4 ppm Rb), corresponding to progressive fractionation of the pegmatite system (Gordienko, 1996). However, these significant variations in Rb concentration were not picked up by in-situ analysis. This apparent discrepancy can be explained by the presence of microinclusions of Rb-bearing minerals, such as muscovite and potassium feldspar, in CGM. Taking into account the structural characteristics of CGM (Ercit, 1994) and the large difference in ionic radius between Rb and cations typically found in the A and B sites in CGM, the incorporation of any significant Rb in the crystal structure seems unlikely.

All generations of CGM contain Li (up to 40 ppm according to the ICP-MS data and up to 22 ppm according to LA-ICP-MS), reflecting the geochemical specialization of the spodumene pegmatites at Kolmozero. The low levels of Li are explained by the late crystallization of CGM relative to spodumene in all parageneses, which removes most of the Li from the mineral-forming environment. In the examined pegmatite system, the concentrations of most of the analyzed trace elements (U, Th, Pb, Zr, W and Ti) in CGM distinctly decrease from the early to late generations: for example, the U content drops from 6063 to

Table 4
Representative analyses of columbite-group minerals from different parageneses of the Kolmozero pegmatite. Major-element oxides in wt.% (by microprobe), trace elements in ppm (by LA-ICP-MS).

	CGM-I						CGM-II			CGM-III			CGM-IV					
	1033	1033	Average	1038	1038	Average	1012	1012	Average	1022	1022	Average	1607	1607	Average	1067	1067	Average
	173	177	n = 15	68	61	n = 16	83	85	n = 7	216	213	n = 23	163	168	n = 8	97	101	n = 14
MnO	9.77	9.46	**10.24**	10.55	9.73	**10.11**	7.39	8.92	**7.90**	12.39	9.15	**11.85**	12.43	12.96	**12.45**	10.53	8.96	**8.84**
TiO$_2$	0.707	0.569	**0.684**	0.716	0.550	**0.602**	0.419	0.313	**0.381**	0.400	0.123	**0.331**	0.185	0.187	**0.182**	0.203	0.153	**0.222**
FeO	11.03	10.22	**9.87**	7.49	8.44	**7.71**	10.44	7.36	**8.54**	4.20	3.09	**3.73**	5.42	2.89	**4.58**	4.71	2.07	**3.48**
Ta$_2$O$_5$	19.28	22.59	**21.31**	29.04	31.17	**29.37**	32.04	46.61	**40.50**	48.23	77.21	**53.84**	45.68	59.79	**54.43**	54.40	86.05	**75.75**
Nb$_2$O$_5$	58.72	56.74	**57.42**	51.76	49.70	**51.71**	49.43	36.59	**42.42**	34.42	10.36	**30.01**	36.19	24.03	**28.49**	30.06	2.62	**11.50**
SnO$_2$	0.082	0.071	**0.084**	0.133	0.115	**0.119**	0.056	0.040	**0.057**	0.206	0.039	**0.145**	0.043	0.024	**0.035**	0.047	0.086	**0.158**
WO$_3$	0.414	0.358	**0.400**	0.311	0.301	**0.311**	0.220	0.169	**0.194**	0.161	0.021	**0.095**	0.061	0.116	**0.109**	0.044	0.059	**0.044**
ppm																		
Mg	129	212	**125**	66	76	**74**	196	193	**208**	61	54	**55**	110	58	**121**	188	30	**135**
Al	93	69	**36**	18	28	**28**	60	17	**66**	11	11	**21**	17	9	**12**	20	68	**286**
Li	20	11	**17**	22	12	**14**	12	5	**7**	22	10	**16**	dl	dl	**dl**	7	dl	**4**
Rb	dl	dl	**dl**	dl	dl	**dl**	dl	dl	**dl**	dl	dl	**dl**	dl	dl	**dl**	dl	dl	**dl**
Sr	1.25	0.76	**0.83**	3.40	0.99	**1.32**	1.75	1.30	**1.99**	0.84	0.78	**4.03**	4.32	2.63	**1.76**	6.84	1.14	**7.29**
Ba	2.91	1.05	**0.59**	dl	dl	**0.40**	0.99	0.46	**1.72**	dl	0.20	**1.25**	0.56	1.42	**0.21**	0.53	0.25	**0.79**
U	933	372	**529**	6063	393	**1065**	90.1	82.3	**85.1**	274	89.3	**226.8**	90.1	5.6	**46.6**	69.3	52.5	**62.4**
Th	15.51	7.32	**13.27**	194.27	14.35	**35.5**	5.22	3.31	**4.04**	5.31	1.09	**4.54**	0.59	10.99	**2.82**	1.62	3.30	**3.28**
Pb	368	160	**278**	1977	217	**398**	35.1	37.5	**36.8**	113.3	130.0	**129.8**	48.2	4.3	**23.0**	26.2	29.3	**28.5**
Tl	0.29	0.13	**8.96**	86.71	13.31	**13.51**	0.038	0.115	**1.301**	0.018	2.584	**4.788**	0.152	0.035	**0.290**	0.677	0.081	**0.082**
Bi	4.934	0.272	**0.543**	2.864	0.423	**0.718**	0.919	0.278	**0.738**	0.631	0.958	**0.922**	0.743	0.632	**0.675**	0.563	1.463	**1.404**
Mo	3.00	2.27	**2.64**	2.54	2.92	**2.63**	1.97	1.72	**1.90**	2.06	1.15	**1.89**	1.53	1.95	**1.61**	1.36	0.99	**1.20**
As	2.64	6.26	**2.50**	26.52	dl	**8.10**	3.12	2.94	**2.86**	4.74	2.20	**3.49**	2.07	9.41	**3.36**	3.91	6.11	**9.54**
Sb	0.30	0.30	**0.20**	3.5	0.86	**1.20**	0.71	0.2	**0.25**	0.3	dl	**0.44**	5.32	3.0	**1.28**	2.30	0.2	**1.69**
Sc	6.2	3.0	**4.8**	3.2	3.7	**3.6**	14.2	4.5	**10.0**	0.9	dl	**1.3**	dl	2.1	**1.7**	6.1	0.9	**4.5**
Y	15.44	9.23	**14.67**	81.45	43.12	**47.82**	10.30	0.29	**3.53**	0.29	0.15	**1.22**	0.06	0.98	**0.61**	0.51	0.05	**0.31**
Zr	3264	834	**2509**	3099	2818	**2918**	387	227	**287**	782	204	**622**	307	202	**283**	201	754	**684**
Hf	392	99	**315**	350	476	**439**	60	47	**51**	187	90	**169**	57	132	**89**	66	425	**394**
Zr/Hf	8.33	8.47	**8.07**	8.85	5.92	**6.98**	6.45	4.78	**5.54**	4.18	2.27	**3.67**	5.39	1.54	**3.06**	3.03	1.78	**1.89**
La	1.750	1.182	**0.461**	0.023	0.235	**0.233**	1.095	dl	**0.456**	dl	0.175	**0.233**	0.007	0.006	**dl**	0.009	dl	**0.016**
Ce	1.511	1.264	**0.399**	0.095	dl	**0.072**	1.073	dl	**0.892**	dl	0.197	**0.244**	dl	dl	**dl**	dl	dl	**0.050**
Pr	0.181	0.117	**0.044**	0.036	dl	**dl**	0.282	dl	**0.103**	dl	0.017	**0.015**	dl	dl	**dl**	dl	dl	**0.014**
Nd	0.612	0.325	**0.171**	0.222	0.068	**0.076**	1.110	0.002	**0.426**	dl	0.061	**0.089**	dl	dl	**dl**	0.017	dl	**0.051**
Sm	0.340	0.196	**0.249**	1.571	0.52	**0.544**	0.27	dl	**0.065**	dl	dl	**dl**	0.098	dl	**0.008**	dl	dl	**dl**
Eu	0.015	0.007	**0.003**	dl	dl	**dl**	0.030	dl	**0.003**	dl	dl	**dl**	dl	0.022	**0.008**	dl	dl	**dl**
Gd	0.552	0.300	**0.453**	5.812	2.23	**2.492**	0.63	dl	**0.203**	dl	0.03	**0.034**	dl	dl	**0.005**	dl	dl	**dl**
Tb	0.320	0.186	**0.301**	3.468	1.594	**1.691**	0.291	dl	**0.099**	dl	dl	**0.011**	dl	0.015	**0.006**	dl	dl	**dl**
Dy	2.504	1.562	**2.411**	20.786	9.47	**10.601**	2.20	0.040	**0.763**	0.037	dl	**0.186**	0.095	0.125	**0.085**	0.07	dl	**0.02**
Ho	0.501	0.317	**0.497**	2.204	1.127	**1.247**	0.306	dl	**0.112**	dl	dl	**0.008**	0.012	0.021	**0.008**	dl	dl	**dl**
Er	2.114	1.183	**1.997**	5.026	2.733	**3.096**	0.946	0.038	**0.347**	dl	0.030	**0.066**	0.040	0.098	**0.047**	0.051	dl	**0.031**
Tm	0.503	0.318	**0.494**	0.915	0.565	**0.609**	0.179	dl	**0.064**	dl	dl	**dl**	dl	0.024	**0.005**	dl	dl	**dl**
Yb	5.241	3.345	**5.048**	7.307	5.04	**5.183**	1.83	0.122	**0.731**	dl	dl	**0.03**	0.087	0.228	**0.130**	0.081	dl	**dl**
Lu	0.890	0.580	**0.872**	0.859	0.614	**0.642**	0.267	0.033	**0.115**	dl	dl	**0.006**	0.017	0.046	**0.026**	dl	dl	**dl**
Total	17.033	10.882	**13.401**	48.324	24.194	**26.750**	10.508	0.235	**4.381**	0.037	0.506	**0.922**	0.356	0.584	**0.330**	0.231	–	**0.179**
(La/Yb)$_n$	0.23	0.24	**0.07**	–	0.03	**0.00**	0.41	0.02	**0.53**	0.07	3.79	**2.64**	0.05	0.02	**0.04**	0.08	–	**0.24**
Eu/Eu*	0.11	0.09	**0.05**	0.01	0.01	**0.02**	0.22	0.33	**0.36**	0.49	0.63	**0.52**	–	–	**0.86**	–	–	**0.60**
Ce/Ce*	0.57	0.73	**0.47**	0.54	0.07	**0.29**	0.50	1.89	**1.18**	0.59	0.74	**1.08**	–	–	**0.50**	–	–	**1.35**

dl — below detection limit. Ce/Ce* = Ce$_n$/(La$_n$ × Pr$_n$)$^{0.5}$. analyses highlighted using bold letters stand for averages of several points within different parageneses.

5.6 ppm, Th from 194.3 to 0.59 ppm, Pb from 1977 to 4.3 ppm, and Zr from 3264 to 201 ppm (Fig. 6b, c). According to the ICP-MS data, the W content decreases from 3113 to 332 ppm, and that of Ti from 3779 to 1383 ppm. Titanium enters the columbite structure predominantly as the disordered rutile component (Černý and Ercit, 1985, 1989; Ercit, 1994) i.e. ~1/3 of the Ti enters the A position and ~2/3 is accommodated in the B position, whereas W probably enters the structure as the ferberite or hübnerite component. Correlation between the Ti

and W abundances probably reflects their similar geochemical evolution (both are strongly compatible during the crystallization of granitic melts), rather than any crystal-chemical controls.

The decrease in these and certain other trace elements in the examined CGM can be potentially explained by progressive fractional crystallization (i.e. removal of these elements from the melt), but from our point of view, hydrothermal processes should also be taken into consideration. The effect of these processes is clearly visible in the zoning
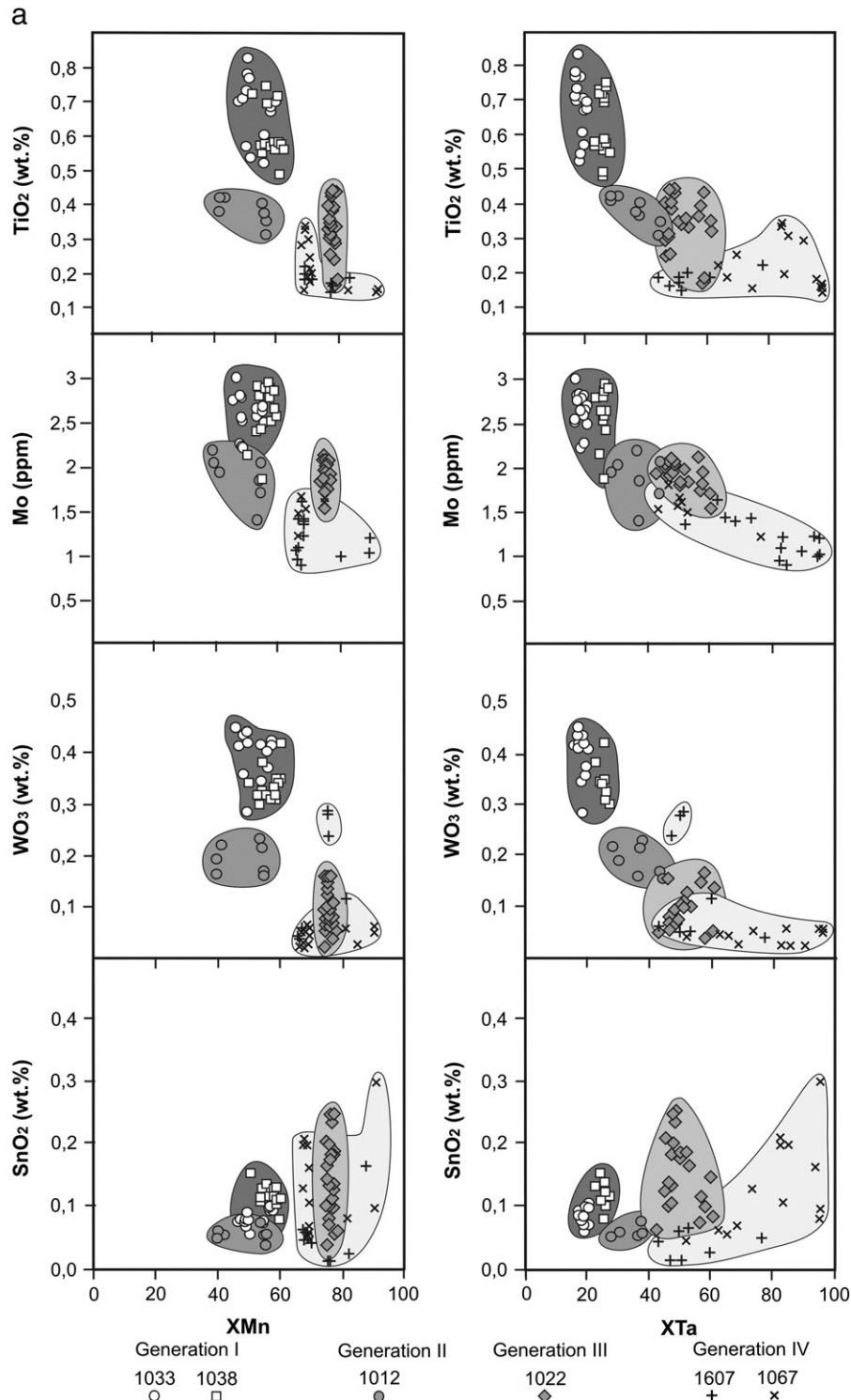
Fig. 6. Diagrams showing variations in XMn and XTa [XMn = 100*Mn/(Mn + Fe) and XTa = 100*Ta/(Ta + Nb), all in atomic per cent] versus selected trace-element abundances, Zr/Hf and Eu/Eu* ratios in CGM; Ti, W and Sn oxide values are in wt.%, other element abundances in ppm. Each field corresponds to a single generation of CGM.
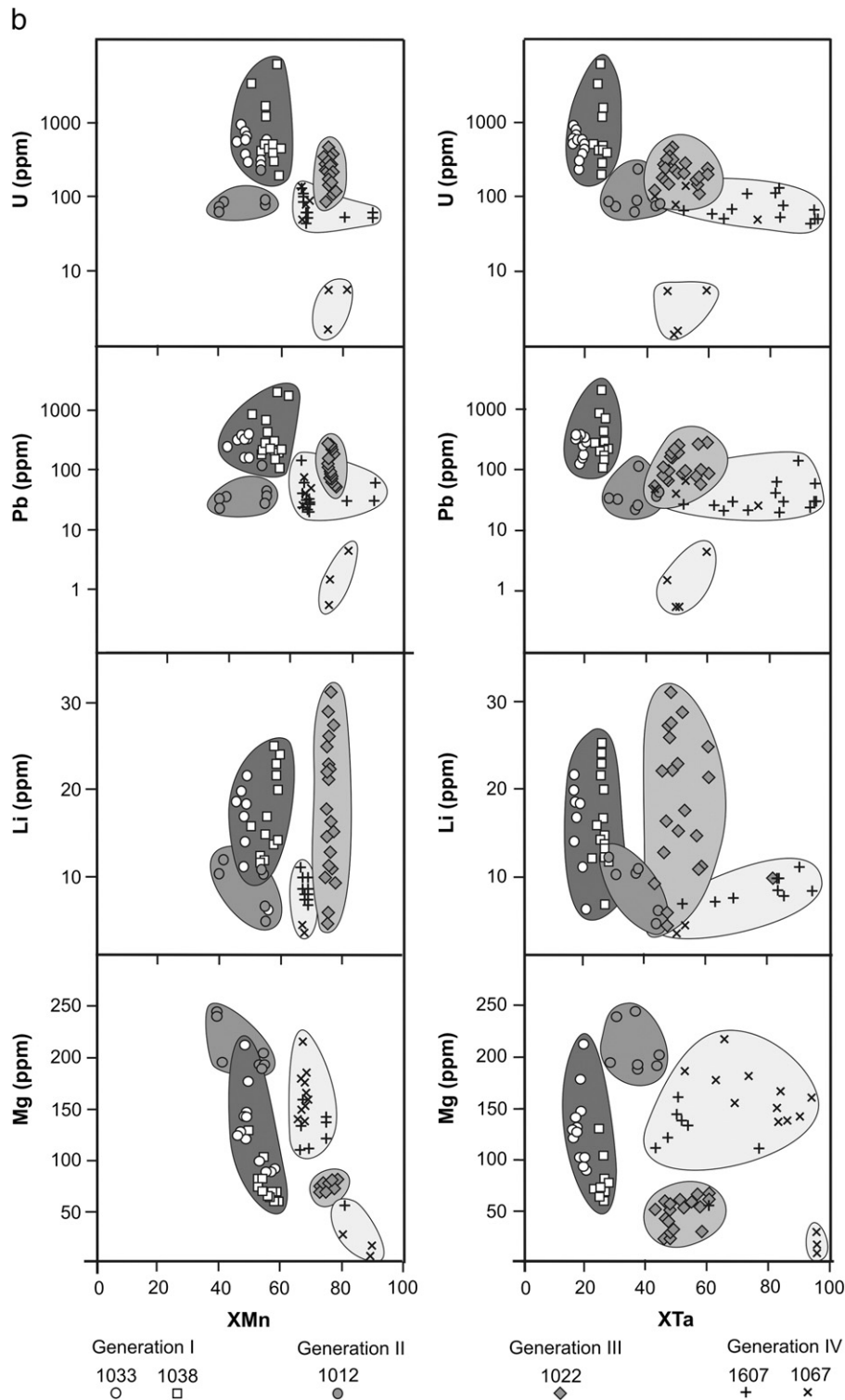
Fig. 6 (*continued*).

patterns exhibited by CGM-IV (Fig. 4i, k). As it was discussed above, CGM-IV was formed in paragenesis with saccharoidal albite in the "secondary aplite" (Gordienko, 1970). The composition of CGM-IV differs drastically from those of the earlier-crystallized CGM generations and is characterized by the lowest concentrations of Zr, U, Th, rare earth elements (REE) and W. Mineralogical evidence for the involvement of hydrothermal processes in the development of almost monomineralic albitite includes the presence of hydrothermal muscovite (sericite),

beryl, spessartine and, especially, sulfides: Cd- and Mn-bearing sphalerite (Gordienko, 1970), pyrite, pyrrhotite, chalcopyrite, bornite, bismuthinite, galena, chalcocite and covellite.

Decreasing concentrations of W in the late generation of CGM possibly reflect removal of this element by fluids as alkali hydrotungstate complexes (Wood and Samson, 2000). Furthermore, W is found as a substituent element in microlite, forming overgrowths on CGM-IV. Concomitantly with the Ti–W-depletion trend, Sn is somewhat enriched in
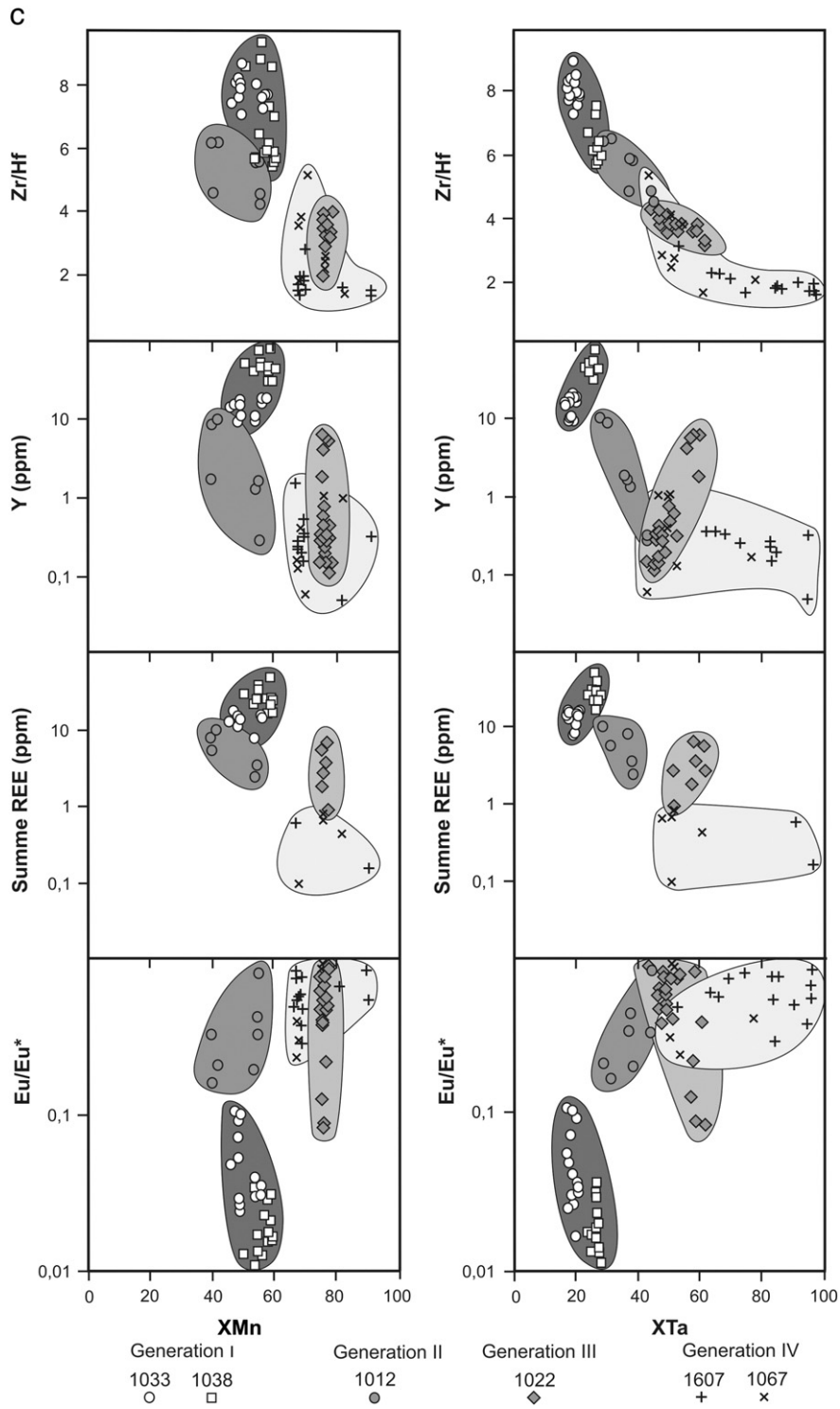
Fig. 6 (*continued*).

CGM-III and -IV (up to 0.3 wt.% SnO$_2$) relative to the earlier-crystallized generations (0.04 to 0.16 wt.% SnO$_2$). Uranium and Pb occur at similar concentration levels and show similar distribution in most CGM generations with the exception of CGM-I, which is characterized by unusually high concentrations of U and Th (up to 6063 and 194 ppm, respectively). The latest generation is less variable in these elements (6–274 ppm U and 0.6–11 ppm Th), in contrast to its highly variable Ta contents. The progressive decrease in the concentrations of these

elements could be explained by the exclusion of large U and Th cations from the columbite structure, which is supported by the presence of uraninite inclusions only in the early generations of CGM. Low U concentrations in the late CGM generations can be explained by the development of microlite overgrowths on CGM-IV.

The first generation of CGM is characterized by the highest contents of Zr (up to 3264 ppm) and Hf (up to 476 ppm) in comparison with the later generations (201–754 ppm Zr and 57–425 ppm Hf), with the

exception of CGM-IVb, which is a product of replacement of the earlier-precipitated CGM. The concentrations of Zr and Hf are greatly variable within each generation, but there is significant overlap of the individual compositional fields with respect to their Zr/Hf ratios, which range from 1.5 to 8.9 (Fig. 6c). The Zr/Hf ratio in these minerals is most probably controlled by zircon fractionation (Linnen and Keppler, 2002; Van Lichtervelde et al., 2007). At Kolmozero, zircon is quite rare, occurring as an accessory mineral in association with CGM-I and CGM-IIb. The mineral forms overgrowths, which indicates its later crystallization relative to the CGM. Zircon also occurs in fine-grained apatite in association with saccharoidal albite in the CGM-IV paragenesis; this generation is characterized by high Hf concentrations (up to 6 wt.% HfO$_2$; Gordienko, 1970).

On the basis of the documented trace element distribution, CGM-I takes a special position in the evolutionary history of the Kolmozero pegmatites because it does not generally show a gradual compositional transition into the later-crystallized generations. The composition of CGM-I suggests that the mechanism of its crystallization was different compared to the other three generations; CGM-I probably precipitated directly from a residual pegmatitic melt. This is indicated by the following mineralogical evidence:

(1) The position of the CGM-I field in compositional diagrams (Fig. 6a–c) is discrete (with minor overlap) with respect to its XTa values, whereas the other generations of CGM form closely overlapping fields.

(2) There is minimal variation in CGM-I chemical composition with respect to Ta.

(3) The highest concentrations of most trace elements are observed in CGM-I, whereas the later generations of CGM are low in these elements, or their concentrations decrease with progressive fractionation. The high trace-element concentrations can be explained by elevated levels of these elements in the evolved pegmatite melt, as supported by the association of CGM-I with specific accessory minerals; for example, high Zr and U concentrations in CGM-I correlate with later crystallization of zircon and uraninite in this paragenesis.
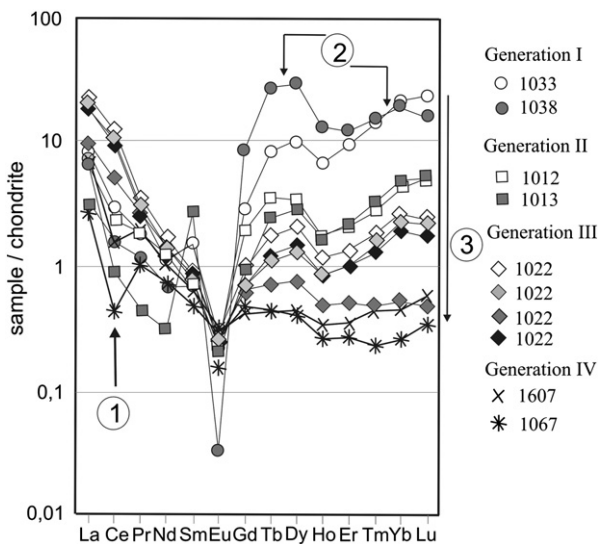

Fig. 7. Chondrite-normalized (Sun and McDonough, 1989) REE patterns in CGM from the differentiated pegmatite body at Kolmozero (ICP-MS data). The numbers in circles show some features of the REE including a negative Ce anomaly (1), disappearance of tetrad effects (2), and decreasing of HREE levels (3).

The data presented above indicate that the behavior of trace elements in CGM depends on the following factors: (a) changes in element concentration in the mineral-forming environment during fractional crystallization; (b) element partitioning between melts and fluids; and (c) redistribution of the element in the host-mineral during its post-magmatic evolution (e.g., due to exsolution).

6.2.3. Mineral chemistry of CGM: REE patterns

The early-crystallizing columbite (CGM-I) formed simultaneously with, or immediately after the major rock-forming minerals microcline, albite, spodumene and muscovite. The large negative Eu anomaly in CGM-I is caused by feldspar fractionation, whereas other REE are not likely to be affected significantly (e.g., Rushmer and Knesel, 2011). Garnet crystallized later during the evolution of pegmatite and is responsible for the decrease in heavy REE (HREE) observed in CGM-II and especially in CGM-III (Fig. 8). A decrease in the content of light REE (LREE) is observed in CGM-IV, which is explained by their partitioning into microlite, which also precipitated at this stage of pegmatite formation. As noted above, zircon is a rare mineral in the Kolmozero albite–spodumene pegmatites and does not play any important role in their REE budget.

The total REE and Y concentrations in the CGM from Kolmozero are quite variable, but generally decrease from 48.3 and 81.5 ppm, respectively, in CGM-I to 0.18 and 0.05 ppm in CGM-IV (Figs. 6c, 7 and 8; Tables 3 and 4). Whereas LREE show little variation, HREE are characterized by variations on the order of two orders of magnitude, which is reflected in their extremely variable (La/Nb)$_n$ ratios (0.3–17.0, although the highest values are observed only in the ICP-MS data for CGM-II and CGM-IV). The latter elements enter the A site in the columbite structure as either the samarskite or euxenite component (Ercit, 1994). The magnitude of the negative Eu anomaly (see above), measured as Eu/Eu*, ranges from 0.01 to 0.86 in different generations of CGM. The documented variations in REE distribution evolve systematically from the early generations of CGM to the late ones and could be used as geochemical markers of pegmatite evolution. The highest total concentrations of REE are observed in CGM-I. These elevated concentrations probably derive from a highly differentiated volatile-rich granitic melt. This origin is supported by "bird-like" normalized REE profiles, with a strong negative Eu anomaly (Eu/Eu* = 0.01–0.11) and M-shaped tetrad effects in the HREE part of the profile, including Gd–Ho (1.1–1.7) and Er–Lu (0.18–0.25). These features are much less conspicuous in the later-crystallized CGM: HREE and Y levels decrease dramatically to 0.82 ppm, as also do the intensity of tetrad effects, Eu anomaly and (Sm/Nd)$_n$ ratio.

The latest generation to crystallize (CGM-IV) lacks the above features: its REE patterns are flatter, (La/Yb)$_n$ ratios are higher (up to 16.9, according to the ICP-MS data, Table 3), the Eu anomaly is less pronounced (up to 0.71), and a negative Ce anomaly is present in some samples (Fig. 7). This generation of CGM is associated with anchimonomineralic aggregates of saccharoidal albite, which is the latest pegmatite paragenesis to crystallize developed by metasomatic replacement. Based on this evidence, the REE distribution pattern of CGM-IV reflects the chemistry of late fluids involved in hydrothermal–metasomatic reworking of the pegmatite. The distribution of other trace elements in CGM-IV also supports this interpretation. The late tantalite-(Mn) (Fig. 8) is depleted in LREE (total REE up to 0.58 ppm) probably due to its co-crystallization with microlite containing high levels of REE.

Interpretation of REE distribution in the Kolmozero CGM is consistent with the evolutionary stages distinguished on the basis of the major-element variations (Figs. 5 and 8). For example, sample 1012 with a wide variation of Ta and Nb contents within a single grain shows enrichment in REE in the more Nb-rich central zone. Some differences between the REE patterns collected by ICP-MS and LA-ICP-MS for the tantalite-(Mn) sample (CGM-IV 1607) stem from differences in relative volumetric contribution of compositionally distinct zones within
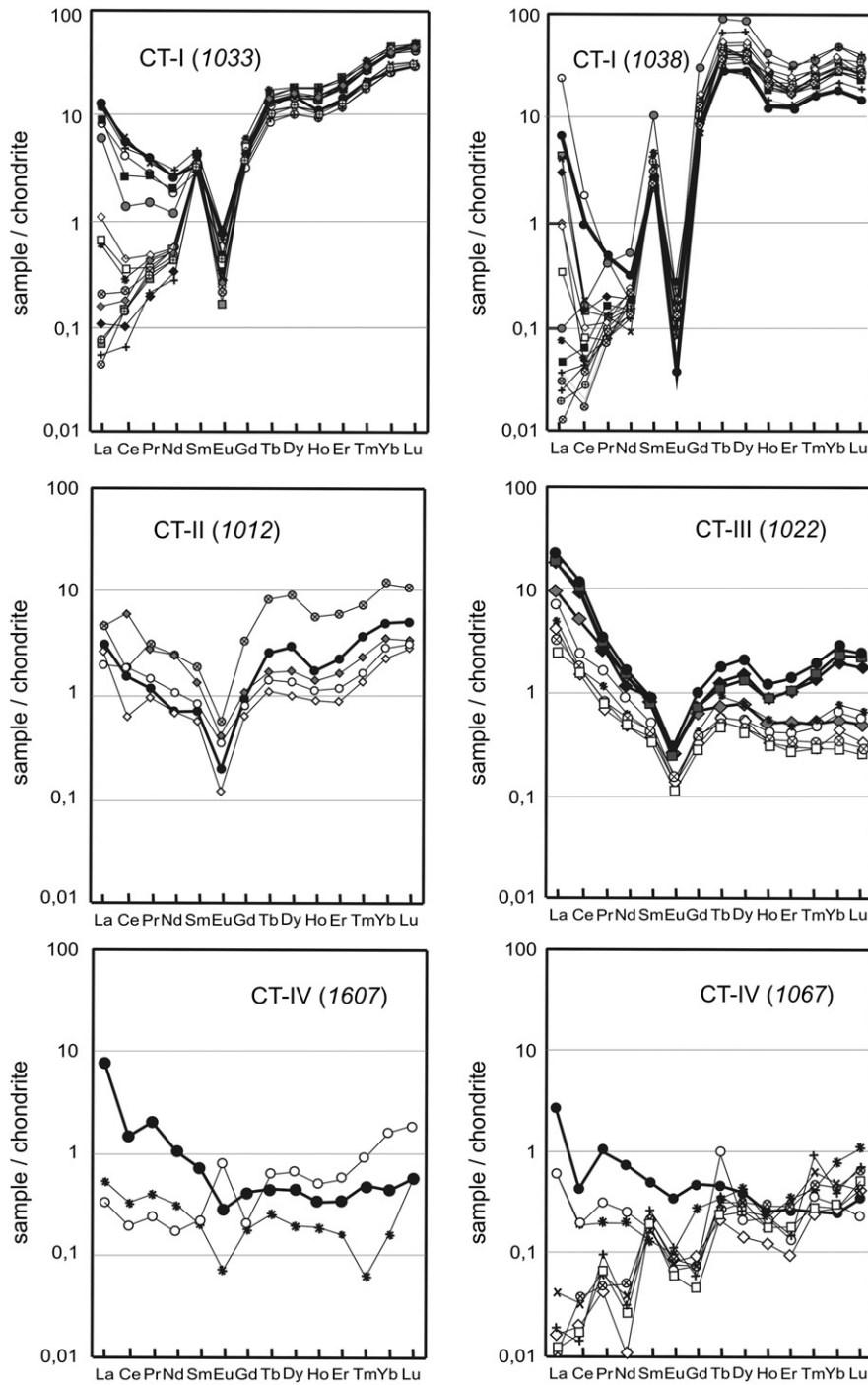
Fig. 8. Chondrite-normalized (Sun and McDonough, 1989) REE patterns of CGM from the differentiated pegmatite body at Kolmozero, ICP-MS data (thick lines) and LA-ICP-MS data (thin lines).

the sample. The most Ta-rich zones correlate with the most irregular REE patterns because element concentrations in these zones approach the detection limit. In terms of the classification developed by Graupner et al. (2010), the chondrite-normalized REE patterns of the Kolmozero samples correspond to groups 1 (CGM-I and -II) and 5 (CGM-III and -IV).

The data obtained in the present work indicate that variations in REE budget among the different generations of CGM from the Kolmozero pegmatites arise from a combination of fractional crystallization early in the evolution of the pegmatite system with an increasing contribution from volatile components at the later stages

as the system was affected by post-magmatic fluid activity (Badanina et al., 2006).

7. Conclusions

1. In this study, we identified several generations of CGM from different parageneses in albite–spodumene pegmatites at Kolmozero (Kola Peninsula), which represent a classical example of Li pegmatite showing no enrichment of Cs or F.
2. Different generations of CGM are characterized by different zoning patterns and great variations in major-element composition. The

early generations are either homogeneous or characterized by (progressive) oscillatory zoning. Černý et al. (1992) interpreted these features as primary magmatic. The latest generation of CGM to crystallize (CGM-IV) is characterized by patchy zoning indicative of metasomatic replacement (Černý et al., 1986; Van Lichtervelde et al., 2007). The early generations of CGM demonstrate a continuous evolutionary trend involving first a decrease in Fe content relative to Mn, then an increase in Ta at decreasing Nb content, and at the final stage of their evolution, a simultaneous increase in Mn and Ta. The latest generation of CGM is tantalite-(Mn), observed as patches in the earlier-crystallized CGM, and occupying a distinct compositional field in a Ta/(Ta + Nb) versus Mn/(Mn + Fe) diagram.

3. During the evolution of the Kolmozero pegmatite system, the concentrations of Ti and W in CGM decreased quite significantly from the early towards the late generations of CGM, whereas Sn shows the opposite trend. Uranium and Pb behaved similarly throughout the entire evolutionary history of the pegmatite system. Only CGM-I exhibits high concentrations of both elements and contains visible uraninite inclusions. The decreasing concentrations of these elements in the late generations of CGM can be explained by crystallization of microlite.

4. The earliest generation of CGM shows trace-element distributions distinct from any of the later generations (with only minor overlap), which indicates that CGM-I crystallized directly from residual pegmatitic melts.

5. The Zr/Hf ratio in the Kolmozero CGM was most probably controlled by zircon fractionation.

6. For the first time, we demonstrate that variations in the concentrations of REE among the different generations of CGM (analyzed by both solution ICP-MS and LA-ICP-MS) reflect progressive stages of the evolution of a pegmatite-forming system. At Kolmozero, the major trends are decreasing total REE and Y contents due to removal of HREE and Y, changes in the magnitude of negative Eu anomalies and tetrad-effect parameters (mostly for Gd–Ho), and gradual flattening of chondrite-normalized REE patterns generally showing a "bird-like" geometry. All these features are typical of late differentiates from granitic volatile-rich magmas. The late metasomatic tantalite-(Mn) is characterized by sharp changes in its REE budget: low REE totals, flat normalized patterns, the absence of Eu anomaly and tetrad effects, and the appearance of a negative Ce anomaly.

On the basis of the mineralogical evidence presented above, we conclude that the evolution of the Kolmozero pegmatites involved two principal stages: an early magmatic stage, divided into two sub-stages (crystallization and recrystallization), and a late hydrothermal–metasomatic stage. This interpretation is in accordance with published experimental data on the solubilities of CGM in silicate melts (Chevychelov, 1998; Linnen and Cuney, 2005).

Acknowledgments

References

Apollonov, V.N., 1999. Mechanism and grow conditions of rhythmical-building crystals. Dokl. Akad. Nauk 364 (1), 94–96 (in Russian).

Aseri, A., Linnen, R.L., 2011. Effects of fluorine on the solubility of Nb, Ta, Zr and Hf in highly fluxed water saturated haplogranitic melts. Mineral. Mag. 75, 458.

Aurisicchio, C., De Vito, C., Ferrini, V., Orlandi, P., 2002. Nb and Ta oxide minerals in the Fonte del Prete granitic pegmatite dike, Island of Elba Italy. Can. Mineral. 40, 799–814.

Badanina, E.V., Trumbull, R.B., Dulski, P., Wiedenbeck, M., Veksler, I.V., Syritso, L.F., 2006. The behavior of rare-earth and lithophile trace elements in rare-metal granites: a study of fluorite, melt inclusions and host rocks from the Khangilay complex, Transbaikalia Russia. Can. Mineral. 44, 667–692.

Beurlen, H., Da Silva, M.R.R., Thomas, R., Soares, D.R., Olivier, P., 2008. Nb–Ta–(Ti–Sn) oxide mineral chemistry as tracer of rare element granitic pegmatite fractionation in the Borborema Province, Northeastern Brazil. Mineral. Deposita 43, 207–228.

Černý, P., 1989. Characteristics of pegmatite deposits of tantalum. In: Möller, P., Černý, P., Saupe, F. (Eds.), Lanthanides Tantalum and Niobium. Springer Verlag, Heidelberg, pp. 192–236.

Černý, P., 1991. Rare-element granite pegmatites I. Anatomy and internal evolution of pegmatite deposits. Geosci. Can. 18, 49–67.

Černý, P., Ercit, T.S., 1985. Some recent advances in the mineralogy and geochemistry of Nb and Ta in rare-element granitic pegmatites. Bull. Mineral. 108, 499–532.

Černý, P., Ercit, T.S., 1989. Mineralogy of niobium and tantalum: crystal chemical relationships, paragenetic aspects and their economic implications. In: Moller, P., Cerny, P., Saupe, F. (Eds.), Lanthanides, Tantalum and Niobium. Springer Verlag, Heidelberg, pp. 27–79.

Černý, P., Goad, B.E., Hawthorne, F.C., Chapman, R., 1986. Fractionation trends the Nb- and Ta-bearing oxide minerals in the Greer Lake pegmatitic granite and its pegmatite aureole, south-eastern Manitoba. Am. Mineral. 71, 501–517.

Černý, P., Novak, M., Chapman, R., 1992. Effects of sillimanite-grade metamorphism and shearing on Nb–Ta oxide minerals in granitic pegmatites: Marsikov, northern Moravia Czechoslovakia. Can. Mineral. 30, 699–718.

Černý, P., Chapman, R., Ferreira, K., Smeds, S.-A., 2004. Geochemistry of oxide minerals of Nb, Ta, Sn and Sb in the Varutrask granitic pegmatite, Sweden: the case of an "anomalous" columbite–tantalite trend. Am. Mineral. 89, 505–518.

Černý, P., Ercit, T.S., Smeds, S.-A., Groat, L.A., Chapman, R., 2007. Zirconium and hafnium in minerals of the columbite and wodginite groups from granitic pegmatites. Can. Mineral. 45, 185–202.

Chevychelov, V.Yu, 1998. Influence of granite composition on behavior of ore metals (W, Mo, Pb, Zn) and petrogenic components in the system alumosilicate melt–aqueous fluid. In: Zharikov, V.A. (Ed.), Experimental and Theoretical Modeling of Mineral Forming Processes. Nauka, Moscow, pp. 118–130 (in Russian).

Ercit, T.S., 1994. The geochemistry and crystal chemistry of columbite-group minerals from granitic pegmatites, southwestern Grenville province, Canadian shield. Can. Mineral. 32, 421–438.

Ercit, T.S., Wise, M.A., Černý, P., 1995. Compositional and structural systematics of the columbite group. Am. Mineral. 80, 613–619.

Fiege, A., Kirchner, C., Holtz, F., Linnen, R.L., Dziony, W., 2011. Influence of fluorine on the solubility of manganotantalite (MnTa2O6) and manganocolumbite (MnNb2O6) in granitic melts — an experimental study. Lithos 122, 165–174.

Gäbler, H.-E., Melcher, F., Graupner, T., Bahr, A., Sitnikova, M.A., Henjes-Kunst, F., Oberthür, T., Brätz, H., Gerdes, A., 2011. Speeding up the analytical workflow for coltan fingerprinting by an integrated Mineral Liberation Analysis/ LA-ICP-MS approach. Geostand. Geoanal. Res. 35, 431–448.

Gordienko, V.V., 1970. Mineralogy, Geochemistry and Genesis of Spodumene Pegmatites. Nauka, Moscow, 240 pp. (in Russian).

Gordienko, V.V., 1996. Granite Pegmatites. SPbGU, St.Petersburg, (272 pp. (in Russian)).

Gordienko, V.V., Krivovichev, V.G., Syritso, L.F., 1987. Metasomitites of Pegmatite Fields. LGU, Leningrad, (221 pp. (in Russian)).

Granitic pegmatites, 1997. In: Shmakin, B.M. (Ed.), Rare-metal pegmatites. Siberian Branch Russ. Acad. Sci., vol. 2. Nauka, Novosibirsk (278 pp. (in Russian)).

Graupner, T., Melcher, F., Gäbler, H.-E., Sitnikova, M., Brätz, H., Bahr, A., 2010. Rare earth element geochmemistry of columbite-group minerals: LA-ICP-MS data. Mineral. Mag. 74, 691–713.

Holten, T., Jamtveit, B., Meakin, P., Cortini, M., Blundy, J., Austrheim, H., 1997. Statistical characteristics and origin of oscillatory zoning in crystal. Am. Mineral. 82, 596–606.

Kudryashov, N.M., Gavrilenko, B.V., Apanasevich, E.A., 2004. Time of formation of rare metal pegmatites in the Kolmozero–Voronja Greenstone Belt (Kola region of the Baltic Shield): U–Pb, Pb–Pb tantalite, columbite and tourmaline dating. Abstr. 32nd IGC Intern. Geol. Congr, pp. 237–238.

Lahti, S.I., 1987. Zoning in columbite–tantalite crystals from the granitic pegmatites of the Erajarve area, southern Finland. Geochem. Cosmochim. Acta 51, 509–517.

Linnen, R.L., Cuney, M., 2005. Granite-related rare-element deposits and experimental constrains on Ta–Nb–W–Sn–Zr–Hf mineralization. In: Linnen, R.L., Samson, I.M. (Eds.), Rare-element Geochemistry and Mineral Deposits: Geological Association of Canada. GAC Short Course Notes, 17, pp. 45–68.

Linnen, R.L., Keppler, H., 1997. Columbite solubility in granitic melts: consequences for the enrichment and fractionation of Nb and Ta in the Earth's crust. Contrib. Mineral. Petrol. 128, 213–227.

Linnen, R.L., Keppler, H., 2002. Melt composition control of Zr/Hf fractionation in magmatic processes. Geochem. Cosmochem. Acta 66, 3292–3301.

London, D., 2008. Pegmatites. Can. Mineral. Spec. Publ. 10 (347 pp.).

Melcher, F., Graupner, T., Henjes-Kunst, F., Oberthür, T., Sitnikova, M., Gäbler, E., Gerdes, A., Brätz, H., Davis, D., Dewaele, S., 2008. Analytical fingerprint of columbite–tantalite (coltan) mineralization in pegmatites: focus on Africa. Proceed. Ninth Intern. Congr. Appl. Mineral. (ICAM), pp. 615–624.

Monecke, T., Gemell, J.B., Monecke, J., 2002. The tetrad effect in rare earth element distribution patterns: a method of quantification with application to rock and mineral samples from granite-related rare metal deposits. Geochim. Cosmochim. Acta 66, 1185–1196.

Novak, M., Černý, P., 1998. Niobium–tantalum oxide minerals from complex granitic pegmatites in the Moldanubicum, Czech Republic; primary versus secondary compositional trends. Can. Mineral. 36, 659–672.

Novak, M., Černý, P., Uher, P., 2003. Extreme variation and apparent reversal of Nb–Ta fractionation in columbite-group minerals from the Scheibengraben beryl–columbite granitic pegmatite, Marsikov, Czech Republic. Eur. Mineral. 15, 565–574.

Petrovskii, M.N., Vinogradov, A.N., 2002. Geology of late-archean Porosozerskii granite massif (Kola Peninsula). Vestn. MGTU 5 (1), 91–98 (in Russian).

Pozhilenko, V.I., Gavrilenko, B.V., Zhirov, D.V., Zhabin, S.V., 2002. Geology of ore districts of Murmansk region. Kola Sci. Centre Russ. Acad. Sci., Apatity, (359 pp. (in Russian)).

Rushmer, T., Knesel, K., 2011. Defining geochemical signatures and timescales of melting processes in the crust: an experimental tale of melt segregation, migration and emplacement. In: Dosseto, A., Turner, S., Van Orman, J. (Eds.), Timescales of Magmatic Processes. Wiley-Blackwell, UK, pp. 181–211.

Shore, M., Fowler, A.D., 1996. Oscillatory zoning in minerals: a common phenomenon. Can. Mineral. 34, 1111–1126.

Spilde, M.N., Shearer, C.K., 1992. A comparison of tantalum–niobium oxide assemblages in two mineralogically distinct rare-element granitic pegmatites, Black Hills, South Dakota. Can. Mineral. 30, 719–737.

Sun, S.-S., McDonough, W.F., 1989. Chemical and isotopic systematics of oceanic basalts: implications for mantle composition and processes. In: Saunders, A.D., Norry, M.J. (Eds.), Magmatism in the Ocean Basins. Geol. Soc. Spec. Publ. 42, London, pp. 313–345.

Tkachev, A.V., 2011. Evolution of metallogeny of granitic pegmatites associated with orogens throughout geological time. In: Sial, A.N., Bettencourt, J.S., De Campos, C.P., Ferreira, V.P. (Eds.), Granite-related Ore Deposits. Geol. Soc., London, Spec. Publ., 350, pp. 7–23.

Uher, P., Černý, P., Chapman, R., Hatar, J., Miko, O., 1998. Evolution of Nb, Ta-oxide minerals in the Prasiva granitic pegmatites, Slovakia. I. Primary Fe, Ti-rich assemblage. Can. Mineral. 36, 525–534.

Van Lichtervelde, M., Linnen, R., Salvi, S., Beziat, D., 2006. The role of metagabbro raft on tantalum mineralization in the Tanco granitic pegmatite Manitoba. Can. Mineral. 44, 625–644.

Van Lichtervelde, M., Salvi, S., Beziat, D., Linnen, R., 2007. Textural features and chemical evolution in tantalum oxides: magmatic versus hydrothermal origins for Ta mineralization in the Tanco Lower pegmatite, Manitoba Canada. Econ. Geol. 102, 257–276.

Wood, S.A., Samson, I.M., 2000. The hydrothermal geochemistry of tungsten in granitoid environments: I. Relative solubilities of ferberite and scheelite as a function of T, P, pH and mNaCl. Econ. Geol. 95, 143–182.